Indoor Localization with LTE Carrier Phase Measurements and Synthetic Aperture Antenna Array

Ali A. Abdallah, Kimia Shamaei, and Zaher M. Kassas
University of California, Irvine

BIOGRAPHIES

Ali A. Abdallah is a Ph.D student in the Department of Electrical Engineering and Computer Science at the University of California, Irvine and a member of the Autonomous Systems Perception, Intelligence, and Navigation (ASPIN) Laboratory. He received a B.E. in Electrical Engineering from the Lebanese American University (LAU). His current research interests include opportunistic navigation, software-defined radio, long-term evolution (LTE), and indoor localization.

Kimia Shamaei is a Ph.D. Candidate in the Department of Electrical Engineering and Computer Science at the University of California, Irvine and a member of the ASPIN Laboratory. She received her B.S. and M.S. in Electrical Engineering from the University of Tehran. Her current research interests include analysis and modeling of signals of opportunity, software-defined radio, LTE, and multipath mitigation.

Zaher (Zak) M. Kassas is an assistant professor at the University of California, Irvine and director of the ASPIN Laboratory. He received a B.E. in Electrical Engineering from the Lebanese American University, an M.S. in Electrical and Computer Engineering from The Ohio State University, and an M.S.E. in Aerospace Engineering and a Ph.D. in Electrical and Computer Engineering from The University of Texas at Austin. In 2018, he received the National Science Foundation (NSF) Faculty Early Career Development Program (CAREER) award, and in 2019, he received the Office of Naval Research (ONR) Young Investigator Program (YIP) award. His research interests include cyber-physical systems, estimation theory, navigation systems, autonomous vehicles, and intelligent transportation systems.

ABSTRACT

An approach for indoor localization using cellular long-term evolution (LTE) carrier phase measurements, which mitigates multipath is developed. The proposed approach exploits the motion of the receiver to synthesize an antenna array from time-separated elements. The synthesized data received by the synthetic antenna array is processed to suppress multipath via determining the direction-of-arrival (DOA) of incoming LTE signals. The proposed LTE-SAN framework is validated experimentally and compared with a standalone LTE receiver, in which the pedestrian-mounted receiver navigated 126.8 m indoors in 100 seconds, while receiving LTE signals from 6 eNodeBs. The proposed approach exhibited a position root mean-squared error (RMSE) of 3.93 m compared to 7.19 m using the standalone LTE receiver.

I. INTRODUCTION

Recent studies estimate that people spend an overwhelming majority of their time indoors [1]. For example, Americans spend, on average, 90% of their time indoors. As such, indoor localization technology has important societal and economical impacts. On one hand, it could be the difference between life and death in emergency situations (e.g., fire, earthquake, law enforcement, etc.). On the other hand, it could save a considerable amount of lost time and effort in malls, airports, hospitals, and storage facilities.

Despite its importance, no single technology has emerged as a clear winner in solving the indoor localization problem. Sensor-based technology (e.g., lidar [2], sonar [3], inertial measurement unit (IMU) [4], and vision [5]) can only provide local position estimates. Moreover, these sensors tend to be bulky and impractical to mount on a human. Also, these sensors may not function in all environments (e.g., smoke, dark, etc.). Signal-based technology (e.g., active

Preprint of the 2019 ION GNSS+ Conference Miami, FL, September 16–20, 2019

radio frequency identification [6], WiFi [7,8], ultra wideband [9,10], and cellular [11–14]) alleviates the sensor-based technology shortcomings, but some require installing a dedicated infrastructure, while other produce a coarse position estimate.

Among the different signal-based technologies, cellular long-term evolution (LTE) signals appear to be very attractive due to their geometric diversity, abundance, and high bandwidth [15]. More importantly, these signals are received at high carrier-to-noise ratio (C/N_0) indoors, where it was demonstrated that the C/N_0 ranged between 50 and 80 dB-Hz in different indoor conditions [13]. In outdoor environments, cellular LTE signals have been demonstrated to yield meter-level accuracy on ground-vehicle mounted receivers [16–20], and sub-meter-level accuracy on unmanned aerial vehicles (UAVs) [21,22]. In addition, cellular LTE signals have been studied recently for indoor localization. A particle filter was used in [23] with laboratory-emulated LTE signals, assuming synchronized eNodeBs which provided a position root mean-squared error (RMSE) of 5.35 m. In [11], different approaches for extracting the time-of-arrival (TOA) from LTE signals have been evaluated, where the final navigation solution showed a two–dimensional (2–D) position RMSE of 8 m with a 50% circular error probability exploiting 4 base stations (also known as evolved Node Bs or eNodeBs). In [13], LTE carrier phase measurements were fused with an inertial measurement unit (IMU) in a tightly-coupled fashion, producing a 2–D RMSE of 3.52 m over a 109 m indoor trajectory.

There are two main challenges associated with exploiting LTE signals for indoor localization: (1) multipath delays indoors can be small compared to the inverse bandwidth of the signal, which limits methods that rely on the TOA to discriminate multipath from line-of-sight (LOS) and (2) the clock biases of LTE eNodeBs are unknown to the receiver. The second challenge was addressed in [13] by introducing a base/rover framework. This paper addresses the first challenge by proposing a synthetic aperture navigation (SAN) framework to mitigate the effect of multipath signals. One way to differentiate between multipath and LOS signals is through the signals' direction of arrival (DOA); however, this requires a large antenna aperture, which is not practical for personal navigation handheld devices. Synthetic aperture antenna circumvents the need for a large physical antenna. Synthetic aperture antenna captures signals from a moving single-element antenna at different time instants, where measurements taken at different time instants correspond to different antenna positions. The measurements are combined and processed as if they were obtained from an antenna with multiple spatially distributed elements. Antenna arrays (physical or synthetic) offer several advantages: (i) they are not limited by the signal bandwidth to resolve multipath delays since they resolve the DOA of received signals, (ii) they are not limited to cases when the LOS is stronger than multipath signals, and (iii) in the case of synthetic array, there is no need for a large physical antenna; instead, the approach relies on signal processing algorithms to achieve the objective [24].

The SAN algorithm performs the following steps: (i) estimate all paths (LOS and NLOS) in the received signal, (ii) select the LOS among all paths, (iii) beamform to coherently combine LOS contributions and suppress multipath, and finally (iv) process the beamformed signal to estimate the parameters of interest for navigation, such as pseudorange and accumulated carrier phase. SAN has been studied in the literature for different applications. In [25], an optimal approach for detecting global navigation satellite system (GNSS) signals utilizing a single moving antenna operating as a synthetic aperture based on an estimator-correlator approach was presented, and the proposed method resulted in a 6 dB gain over that of a static receiver. In [26], a synthetic antenna array was implemented to reduce GNSS multipath errors in vehicular navigation applications. Simulation results showed that in the presence of one multipath signal and two antenna elements, the proposed method removed multipath effects in all the cases and almost distortionless correlation peaks were obtained.

This paper presents an LTE-SAN approach for indoor localization and validates the performance experimentally in a deep indoor environment over a 126.8 m trajectory traversed in 100 seconds. The achieved 2–D RMSE is demonstrated to be 3.93 m with the proposed LTE-SAN approach, compared to 7.19 m with a state-of-the-art standalone carrier-phase-based LTE receiver.

The remainder of this paper is organized as follows. Section presents the proposed LTE-SAN approach and discuss: (i) the LTE-SAN model, (ii) DOA estimation using estimation of signal parameters via rotational invariance techniques (ESPRIT), (iii) multipath mitigation via Capon's beamformer, and (iv) the navigation filter. Section III validates experimentally the proposed LTE-SAN framework in an indoor environment and compares the performance with standalone LTE approach. Concluding remarks are given in Section IV.

II. SYNTHETIC APERTURE NAVIGATION APPROACH AND BEAMFORMING PROCESS

In this section, multipath mitigation via spatial separation of received LTE signals for a pedestrian indoor localization system is discussed. The spatial separation is performed using a synthetic antenna array. The analysis assumes linear movement of the pedestrian for over a short duration of time $t_{\text{lin}} = KFt_{\text{frame}}$, where K is the is the number of snapshots, F is the number of skipped LTE frames to account for the physical separation between two consecutive snapshots, N is the number of antenna elements which could be any number greater than or equal to one, and t_{frame} is the LTE frame duration defined as $t_{\text{frame}} = 0.01$ seconds. Over this period of time, the pedestrian's speed v_c is assumed to be constant, which is estimated in the navigation filter by taking the average over t_{lin}. The altitude of pedestrian-mounted receiver is estimated using an external sensor (e.g., a barometer). Therefore, only the 2-D position, 2-D velocity, and the azimuth angles $\{\phi_l^{(u)}\}_{l=0}^{L^{(u)}}$ of the impinging signals (both LOS and multipath signals) from the u-th eNodeB are estimated as shown in Fig. 1, where $L^{(u)}$ is the number of multipath components. Fig. 1 illustrates the proposed LTE-SAN approach with a synthetic uniform linear antenna array and shows the user trajectory, the sampling process of the moving antenna, and the azimuth angles impinging on the antenna array from the u-th eNodeB at instant k. The following subsections present the LTE-SAN model, discuss DOA estimation using ESPRIT subspace-based estimator, analyze the beamforming process to mitigate multipath, and formulate the navigation filter.

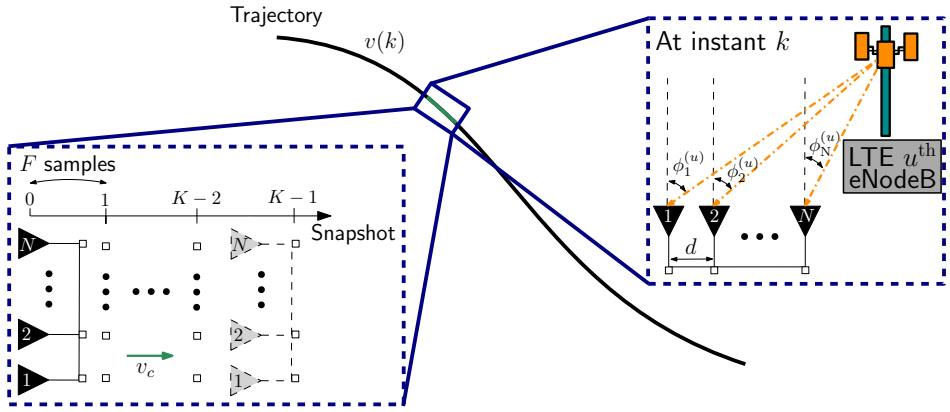

Fig. 1. Synthetic uniform linear array: trajectory, sampling process of the moving antenna, and snapshot of the azimuth angles impinging on the antenna array from the u-th eNodeB at instant k.

A. LTE-SAN Model

This paper assumes that LTE carrier phase measurements are produced by tracking the cell-specific reference signal (CRS) in the received LTE signals using the carrier phase-based software defined receiver developed in [18, 27]. The channel impulse response (CIR) of the k-th received LTE frame is estimated for each sample at the tracking step and will be denoted as $h(k)$. The proposed approach starts at the receiver's post-correlation phase. Hence, the CIR of the CRS is attractive due to high bandwidth of CRS, which is the same as the LTE system bandwidth. Then, the estimated channel frequency response (CFR) of the received LTE signal from the u-th eNodeB at the k-th snapshot can be expressed as

$$h_n^{(u)}(k) = \sum_{l=0}^{L^{(u)}} \alpha_l^{(u)} a_l(\phi_n^{(u)}) e^{-j2\pi f_c \tau_l^{(u)}}, \quad \text{for} \quad n = 1, \cdots, N \quad \text{and} \quad k = 1, \cdots, K, \tag{1}$$

where $\alpha_l^{(u)}$ and $\tau_l^{(u)}$ are the attenuation factor and the delay of the l-th multipath component, f_c is the carrier frequency, and $a_l(\phi_n^{(u)})$ and $a_0(\phi_n^{(u)})$ are the steering elements at the n-th antenna element of the l-th multipath and LOS components, respectively. The steering element determines the spatial representation of the incoming signal. In other words, it represents the phase delay experienced by the antenna element with respect to a specified origin, which is chosen here to be the first antenna element. The LOS steering element of the u-th eNodeB at the n-th

antenna element can be expressed as

$$a_0(\phi_n^{(u)}) = e^{(n-1)j\mu^{(u)}}, \tag{2}$$

where $\mu^{(u)} = -\frac{2\pi}{\lambda} d \sin(\theta_1^{(u)})$, is the spatial frequency for the u-th eNodeB [28]. To simplify notation, the superscript "$^{(u)}$" will be dropped for the rest of the paper. The received signals can be formulated as

$$\boldsymbol{h}(k) = \mathbf{A}(k)\boldsymbol{x}(k) + \boldsymbol{\nu}(k), \tag{3}$$

where $\boldsymbol{\nu}$ is a noise sequence, which is modeled as white Gaussian and spatially uncorrelated with covariance $\sigma^2\mathbf{I}_{N\times N}$ and

$$\mathbf{A}(k) = [\boldsymbol{a}_0(\phi), \cdots, \boldsymbol{a}_L(\phi)], \tag{4}$$

$$\boldsymbol{x}(k) = \left[\alpha_0 e^{-j2\pi f_c \tau_0}, \cdots, \alpha_L e^{-j2\pi f_c \tau_L}\right]^{\mathsf{T}}, \tag{5}$$

where $\boldsymbol{a}_l(\phi)$ and $\boldsymbol{a}_0(\phi)$ are the steering vectors of all N antenna elements of the l-th multipath and LOS components, respectively. The collected data at the K snapshots are stacked as

$$\mathbf{H}^{(K)} = \left[\boldsymbol{h}^{\mathsf{T}}(k), \boldsymbol{h}^{\mathsf{T}}(k+F), \cdots, \boldsymbol{h}^{\mathsf{T}}(k+KF)\right]^{\mathsf{T}}. \tag{6}$$

B. DOA Estimation: Standard ESPRIT

Different DOA estimation techniques exist in the literature, with different performance, resolution, and computational cost. Subspace-based DOA estimation techniques have better resolution than maximum-likelihood (ML) techniques [28]. Subspace approach basically rely on the fact that the spatial covariance matrix (i.e., signals plus noise) of the received data spans two orthogonal subspaces, namely, the signal and noise subspaces, where the signal subspace is spanned by the larger eigenvalues of the data covariance matrix. Multiple Signal Classification (MUSIC) is one of the most popular and early proposed methods for super-resolution DOA estimation [29]. When applied to LTE DOA estimation, MUSIC has yielded high resolution performance [30]. However, MUSIC has a high computational cost. An alternative technique with a low computational cost and high resolution capabilities is the ESPRIT algorithm. ESPRIT requires symmetric geometric pattern and invariance transformation characteristic for the applied antenna design. ESPRIT divides the array into two symmetric subarrays as shown in Fig. 2. The design shown in Fig. 2(a) is the most common structure and adopted in the proposed approach.

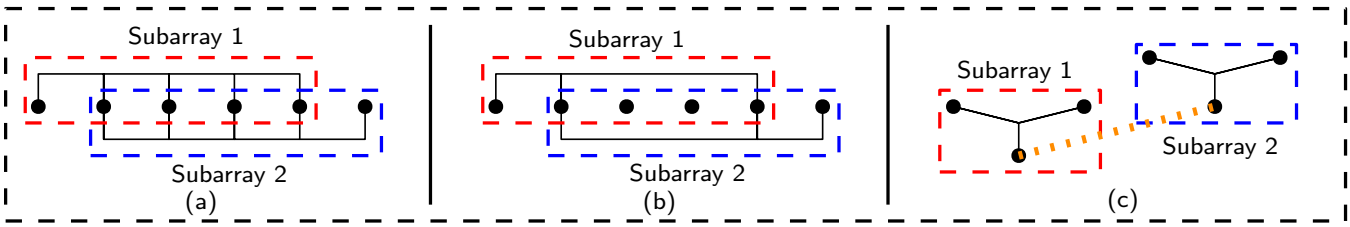

Fig. 2. Different structures of ESPRIT subarrays.

In practice, the spatial covariance matrix $\mathbf{R}_{HH}$ of the received LTE data in (6) is not known; however, an estimate of $\mathbf{R_{HH}}$ could be obtained as

$$\hat{\mathbf{R}}_{HH} = \frac{1}{N_s}\mathbf{H}^{(K)}\mathbf{H}^{(K)\mathsf{H}}, \tag{7}$$

where N_s is the number of samples and $(.)^{\mathsf{H}}$ is the Hermitian operator. Algorithm 1 summarizes the steps of the standard ESPRIT algorithm. Further details about ESPRIT can be found in [31].

B.1 Preprocessing Scheme: Spatial Smoothing

The DOA estimation algorithms described so far assume that the incoming signals are noncoherent. In other words, they assume that the steering matrix is full rank. If the impinging signals are highly correlated or coherent,

Algorithm 1: Standard ESPRIT Algorithm [31]

1. Collect data samples $\mathbf{H}^{(K)}$
2. Estimate the input covariance matrix $\hat{\mathbf{R}}_{HH}$ using (7)
3. Estimate the order of the system $\hat{L}+1$ (see Subsection II-B.2)
4. Perform singular value decomposition $\mathbf{H}^{(K)} = \mathbf{U}\mathbf{\Sigma}\mathbf{V}^{\mathbf{H}}$ and compute $\mathbf{U}_s$ with the $\hat{L}+1$ dominant left singular values
5. Solve using the total least squares approach, the invariance equation

$$\mathbf{J}_1\mathbf{U}_s\mathbf{\Psi} = \mathbf{J}_2\mathbf{U}_s,$$

   where $\mathbf{J}_1 = [\mathbf{I}_{KN-1\times KN-1}\ \mathbf{0}_{KN-1\times 1}]$ and $\mathbf{J}_2 = [\mathbf{0}_{KN-1\times 1}\ \mathbf{I}_{KN-1\times KN-1}]$
6. Calculate the eigenvalues of the resulting complex-valued solution

$$\mathbf{\Psi} = \mathbf{T}\mathbf{\Phi}\mathbf{T}^{-1},$$

   with $\mathbf{\Phi} = \mathrm{diag}[\phi_1, \cdots, \phi_{\mathrm{D}}]$.
7. Extract the angular information via

$$\mu_d = \arg(\phi_d)$$
$$\phi_d = \arcsin\left(-\frac{-\lambda}{2\pi d}\mu_d\right)$$

different DOA estimation techniques will fail to provide reliable DOA estimates due to having an ill-conditioned or even singular spatial covariance matrix. In practical multipath scenarios, having highly correlated signals is very common where the incoming signals are scaled and delayed versions of each other. To overcome this challenge, the data covariance matrix is preprocessed before "feeding" it to the DOA estimation algorithm. Two well-known preprocessing schemes deal with this challenge: (1) Forward-Backward Averaging (FB-averaging) and (2) Spatial Smoothing (SS) [28]. FB-averaging is capable of resolving only the case of two coherent signals [32]. In rich multipath area, the data may encounter more than two coherent signals. This raises the need for a more sophisticated approach to resolve this challenge. To this end, SS seems to be an attractive technique to tackle this issue. SS divides the antenna array into a smaller number of subarrays (denoted C) and the data covariance matrices obtained from each subarray are averaged. For one-dimensional SS, e.g, uniform linear array (ULA) is divided into $N_{sub} = KN - C + 1$ subarrays to decouple the eigenvectors of at most C coherent signals. The mathematical implementation of the new data for SS is expressed as

$$\mathbf{H}_{ss}^{(K)} = \left[\mathbf{H}_{fss}^{(K)}\ \ \mathbf{H}_{bss}^{(K)}\right],$$

where $\mathbf{H}_{fss}^{(K)}$ and $\mathbf{H}_{bss}^{(K)}$ are the forward and the backward spatially smoothed data, defined as

$$\mathbf{H}_{fss}^{(K)} = \left[\mathbf{J}_{f_1}\mathbf{H}^{(K)}\ \ \mathbf{J}_{f_2}\mathbf{H}^{(K)}\ \ \cdots \mathbf{J}_{f_C}\mathbf{H}^{(K)}\right]$$
$$\mathbf{H}_{bss}^{(K)} = \left[\mathbf{J}_{b1}\mathbf{H}^{(K)}\ \ \mathbf{J}_{b2}\mathbf{H}^{(K)}\ \ \cdots \mathbf{J}_{bC}\mathbf{H}^{(K)}\right],$$

and

$$\mathbf{J}_{f_c} = \left[\mathbf{0}_{N_{sub}\times(c-1)}\ \ \mathbf{I}_{N_{sub}}\ \ \mathbf{0}_{N_{sub}\times(KN-N_{sub}-c+1)}\right] \in \mathbb{R}^{N_{sub}\times KN}$$
$$\mathbf{J}_{bc} = \left[\mathbf{0}_{N_{sub}\times(KN-N_{sub}-c+1)}\ \ \mathbf{I}_{N_{sub}}\ \ \mathbf{0}_{N_{sub}\times(c-1)}\right] \in \mathbb{R}^{N_{sub}\times KN}$$
$$\text{for} \qquad c = 1, \cdots, C$$

Then, the corresponding forward and backward spatially smoothed data covariance matrices are obtained as

$$\hat{\mathbf{R}}_{HH}^{fss} = \frac{1}{CN_s}\mathbf{H}_{fss}^{(K)}\mathbf{H}_{fss}^{(K)^{\mathsf{H}}}$$
$$\hat{\mathbf{R}}_{HH}^{bss} = \frac{1}{CN_s}\mathbf{H}_{bss}^{(K)}\mathbf{H}_{bss}^{(K)^{\mathsf{H}}}.$$

Finally, the overall spatially smoothed data covariance matrix is obtained by averaging both the forward and backward subarrays as

$$\hat{\mathbf{R}}_{HH}^{ss} = \frac{1}{2}\left(\hat{\mathbf{R}}_{HH}^{fss} + \hat{\mathbf{R}}_{HH}^{bss}\right).$$

Note that there is a trade-off between the number of coherent signals to be resolved and the new degree of freedom associated with the new subarray's size.

B.2 Model Order Estimators

In addition to the coherence issue of incoming signals, the number of signals $L+1$ impinging on the array was assumed to be known so far. Practically, this number is unknown and has to be estimated from the received data. The simplest way of estimating the number of signals is by estimating the number of repeated small eigenvalues other than the large ones. In other words, if the multiplicity $\hat{q}$ of the smallest eigenvalues is found, an estimate of the number of signals, $\hat{L}+1$, can be obtained directly as

$$\hat{L} = KN - \hat{q} - 1.$$

In practice, the smallest eigenvalues representing the noise power will not be identical. Instead, they will appear as a closely spaced cluster. This could be formed as a detection problem where the number of incoming signals obtained by a ULA is $L \in \{0, 1, \cdots, KN-1\}$. To estimate the order of the system, one can apply the minimum description length criterion (MDL) or Akaike information theoretic criterion (AIC) [33, 34]. The above approaches result in minimizing the following criteria

$$\begin{cases} -\ln\left[\dfrac{\prod_{i=L}^{KN}\lambda_i^{\frac{1}{KN-L-1}}}{\frac{1}{N-L-1}\sum_{i=L+2}^{KN}\lambda_i}\right]^{(KN-L-1)N_s} + \frac{1}{2}\hat{p}(K,N,L)\ln(N_s), & \text{MDL} \\ -\ln\left[\dfrac{\prod_{i=L+2}^{KN}\lambda_i^{\frac{1}{KN-L-1}}}{\frac{1}{KN-L-1}\sum_{i=L+2}^{KN}\lambda_i}\right]^{(KN-D)N_s} + \hat{p}(K,N,L), & \text{AIC}, \end{cases}$$

where $\hat{p}(K,N,L)$ is a function of the number of independent parameters defined as the penalty function [35].

C. Multipath Mitigation: Capon's Beamformer

In order to suppress multipath signals, the only signal that is allowed to pass through the beamformer is the LOS signal. After applying beamforming to the synthetic data, the data received by array elements form a single output as follows

$$\boldsymbol{y}(k) = \boldsymbol{w}^{\mathsf{H}}\mathbf{H}^{(K)}, \tag{8}$$

where $\boldsymbol{w}$ is a weighing vector that is determined by optimizing some objective function subject to certain constraints. Different beamforming methods have different criteria to optimize over. The common strategy behind beamforming is to steer the antenna array in a specified direction at a time and evaluate the specified objective seeking an optimal complex weighting vector to weight the received signals at different snapshots. Herein, the purpose behind the proposed LTE-SAN framework is to suppress the multipath components while passing the beam where the LOS component impinges on the synthetic antenna array. To do so, different beamforming techniques could be applied. A potential beamforming technique is the Capon's method, also known as minimum variance distortionless response

(MVDR) beamformer. The chosen weighting vector for MVDR minimizes the variance of the array output signal while passing the signal arriving from the look direction with no distortion which can be shown to be

$$\boldsymbol{w} = \frac{\hat{\mathbf{R}}_{HH}^{-1}\boldsymbol{a}_0(\phi)}{\boldsymbol{a}_0^{\mathbf{H}}(\phi)\hat{\mathbf{R}}_{HH}^{-1}\boldsymbol{a}_0(\phi)}, \tag{9}$$

where $\boldsymbol{a}_0$ is the LOS steering vector.

D. Navigation Filter: Extended Kalman Filter

An extended Kalman filter (EKF) is used to estimate the state vector from the corrected LTE carrier phase measurements $\boldsymbol{z}^{'}$. The altitude of the navigating receiver is assumed to be obtained using an external sensor (e.g., a barometer). Therefore, only the 2-D position $\boldsymbol{r}$ and velocity $\dot{\boldsymbol{r}}$ are considered. The EKF estimates the vector $\boldsymbol{x}$ defined as

$$\boldsymbol{x} \triangleq \left[\boldsymbol{x}_{\text{ped}}^{\mathsf{T}}, \boldsymbol{x}_{\text{clk}}^{\mathsf{T}}\right]^{\mathsf{T}},$$

with the pedestrian's state vector is defined as $\boldsymbol{x}_{\text{ped}} \triangleq \left[\boldsymbol{r}^{\mathsf{T}}, \dot{\boldsymbol{r}}^{\mathsf{T}}\right]^{\mathsf{T}}$. The clock state vector $\boldsymbol{x}_{\text{clk}}$ is defined as $\boldsymbol{x}_{\text{clk}} \triangleq \left[c\delta t_1, c\dot{\delta} t_1, \cdots, c\delta t_U, c\dot{\delta} t_U\right]^{\mathsf{T}}$, where U is the number of eNodeBs, c is the speed of light, and $\{\delta t_u\}_{u=1}^{U}$ and $\{\dot{\delta} t_u\}_{u=1}^{U}$ are the relative clock bias and drift between the receiver and u-th eNodeB. The pedestrian's motion is assumed to evolve according to a nearly constant velocity dynamics, i.e,

$$\ddot{\boldsymbol{r}}(t) = \tilde{\boldsymbol{w}}(t), \tag{10}$$

where $\tilde{\boldsymbol{w}}$ is a process noise vector, which is modeled as zero-mean white random process with power spectral density $\tilde{\mathbf{Q}}_{\text{ped}} = \text{diag}[\tilde{\text{q}}_{\text{x}}, \tilde{\text{q}}_{\text{y}}]$, where $\tilde{q}_x$ and $\tilde{q}_y$ are the power spectral densities of the acceleration in the $x-$ and $y-$ directions [36]. The clock error dynamics are assumed to evolve according to

$$\dot{\boldsymbol{x}}_{\text{clk}} = \mathbf{A}_{\text{clk}}\boldsymbol{x}_{\text{clk}}(t) + \tilde{\boldsymbol{w}}_{\text{clk}}(t), \tag{11}$$

$$\mathbf{A}_{\text{clk}} = \begin{bmatrix} 0 & 1 \\ 0 & 0 \end{bmatrix}, \qquad \tilde{\boldsymbol{w}}_{\text{clk}} = \begin{bmatrix} \tilde{\boldsymbol{w}}_{\delta t} \\ \tilde{\boldsymbol{w}}_{\dot{\delta} t} \end{bmatrix},$$

where the elements of $\tilde{\boldsymbol{w}}_{\text{clk}}$ are modeled as zero-mean mutually independent white noise processes and the power spectral density of $\tilde{\boldsymbol{w}}_{\text{clk}}$ is $\tilde{\mathbf{Q}} = \text{diag}\left[\text{S}_{\tilde{\text{w}}_{\delta t}}, \text{S}_{\tilde{\text{w}}_{\dot{\delta} t}}\right]$.

III. EXPERIMENTAL RESULTS

This section validates the proposed LTE-SAN framework experimentally in a deep indoor environment and compares the performance with a standalone LTE receiver.

A. Experimental Setup and Environmental Layout

The experiment was performed in the Engineering Gateway building at the University of California, Irvine, USA. A quad-channel National Instrument (NI) universal software radio peripheral (USRP)-2955 was connected to the pedestrian-mounted receiver to sample LTE signals with a sampling rate of 10 MSps. The receiver was equipped with 4 consumer-grade cellular omnidirectional Laird antennas. The USRP was tuned to 4 different carrier frequencies and was listening to 6 eNodeBs from 3 U.S. cellular providers whose characteristics are summarized in Table I. The sampled LTE signals were transferred from the USRP-2955 via a PCI Express cable and stored on a laptop for post-processing. Fig. 3 shows the environment layout in which the experiment was performed, the positions of the eNodeBs from which signals were collected, and the experimental hardware and software setup.

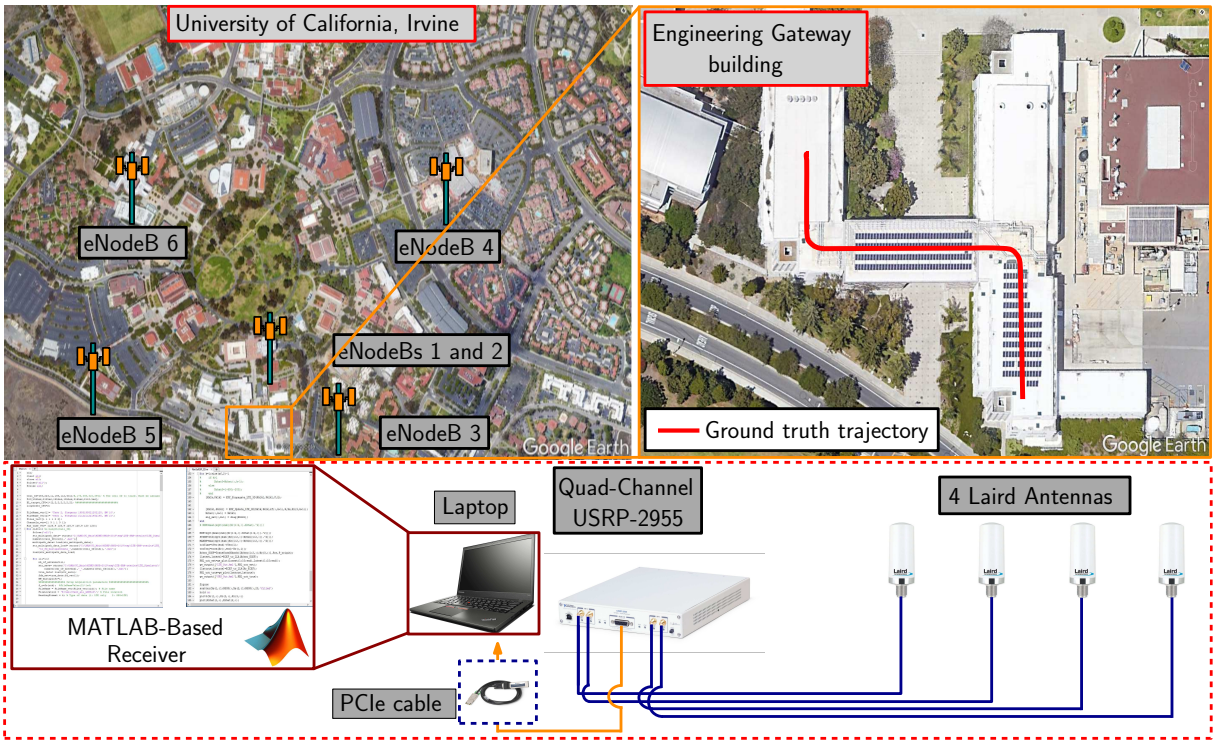

Fig. 3. Environmental layout and experimental setup. The top left subfigure shows the positions of the LTE eNodeBs. The top right subfigure shows the Engineering Gateway building where the experiment was performed along with the ground truth trajectory. The bottom subfigure shows the experimental setup.

TABLE I
LTE ENODEBS' CHARACTERISTICS

eNodeB	Carrier frequency (MHz)	N_{ID}^{Cell}	Bandwidth (MHz)	Cellular provider
1	1955	93	20	AT&T
2	2125	223	20	Verizon
3	1955	11	20	AT&T
4	1955	198	20	AT&T
5	2145	112	20	T-Mobile
6	2112.5	401	20	AT&T

B. Navigation Solution

The pedestrian traversed 126.8 m in 100 seconds. The pedestrian's position and velocity state vectors were initialized using a multi-variate Gaussian random vector generator with the true state vector $\boldsymbol{x}_{\text{ped}} = [0, 0, 1.12, 0]$ as the mean and initial covariance matrix chosen to be $\mathbf{P}_{\text{ped}}(0) = \text{diag}[25, 25, 10, 10]$, which is reasonable, assuming that GPS was available before entering the building. The initial position is used to initialize the relative clock biases with uncertainty 25 m^2. The measurement noise variance $\left\{\sigma^2{}_{v_u}\right\}_{u=1}^{U=6}$ were set to $\left\{c^2 \frac{\alpha_u}{(C/N_0)_u}\right\}_{u=1}^{U=6}$, respectively, where $(C/N_0)_u$ is the received C/N_0 for the u-th eNodeB and $\{\alpha_u > 0\}_{u=1}^{U}$ are tuning parameters that were chosen to be $\{3.74, 2.53, 4.12, 5.87, 5.52, 8.94\} \times 10^{-12}$ in this paper.

Fig. 4 shows the receiver's ground truth trajectory versus the navigation solution from: (1) standalone LTE and (2) the proposed LTE-SAN framework. The ground truth was obtained with a camera that was mounted on the moving cart, which was pushed by the pedestrian to record the location of specific landmarks in the environment with known locations. Table II summarizes the experimental results. It can be seen that the proposed LTE-SAN

TABLE II
INDOOR LOCALIZATION PERFORMANCE COMPARISON

Performance Measure [m]	**Standalone LTE**	**LTE-SAN**
RMSE	7.19	3.93
Standard deviation	3.32	1.65
Maximum error	12.89	5.63

framework outperformed the LTE standalone solution with a position RMSE of 3.93 m versus 7.19 m respectively.

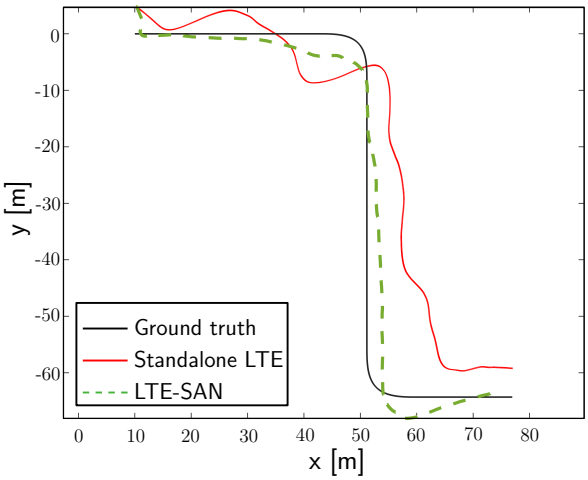

Fig. 4. The pedestrian's ground truth trajectory versus the navigation solution from: (1) standalone LTE and (2) LTE-SAN.

IV. CONCLUSION

This paper presented a practical and feasible approach to spatially separate LOS from multipath signals in a pedestrian indoor localization system that uses LTE carrier phase measurements. The four steps of performing a beamforming process were discussed: preprocessing filtering, model order estimation, DOA estimation, and weighting vector generation. The standard ESPRIT algorithm was applied to estimate DOA in the proposed LTE-SAN framework. An experiment was performed to demonstrate the efficacy of the proposed framework, where the pedestrian traversed 126.8 m in 100 seconds in a deep indoor environment, while listening to 6 cellular LTE eNodeBs. The proposed LTE-SAN framework exhibited position RMSE of 3.93 m compared with 7.19 m from a standalone LTE receiver.

ACKNOWLEDGMENT

This work was performed under the financial assistance award 70NANB17H192 from U.S. Department of Commerce, the National Institute of Standards and Technology (NIST). The authors would like to thank Mohamad Orabi, Zainab Ashai, and Joe Khalife for their help in data collection.

References

[1] Indoor air quality. [Online]. Available: https://www.epa.gov/

[2] M. Atia, S. Liu, H. Nematallah, T. Karamat, and A. Noureldin, "Integrated indoor navigation system for ground vehicles with automatic 3-D alignment and position initialization," *IEEE Transactions on Vehicular Technology*, vol. 64, no. 4, pp. 1279–1292, April 2015.

[3] J. Steckel, A. Boen, and H. Peremans, "Broadband 3-D sonar system using a sparse array for indoor navigation," *IEEE Transactions on Robotics*, vol. 29, no. 1, pp. 161–171, February 2013.

[4] Y. Wang, S. Askari, and A. M. Shkel, "Study on mounting position of IMU for better accuracy of ZUPT-aided pedestrian inertial navigation," in *IEEE International Symposium on Inertial Sensors and Systems*, April 2019, pp. 1–4.

[5] C. Zhu, G. Giorgi, and C. Gunther, "Planar pose estimation using a camera and single-station ranging measurements," in *Proceedings of ION GNSS Conference*, September 2017.

[6] S. Saab and Z. Nakad, "A standalone RFID indoor positioning system using passive tags," *IEEE Transactions on Industrial Electronics*, vol. 58, no. 5, pp. 1961–1970, May 2011.

[7] C. Yang and H. Shao, "WiFi-based indoor positioning," *IEEE Communications Magazine*, vol. 53, no. 3, pp. 150–157, March 2015.

[8] J. Khalife, Z. Kassas, and S. Saab, "Indoor localization based on floor plans and power maps: Non-line of sight to virtual line of sight," in *Proceedings of ION GNSS Conference*, September 2015, pp. 2291–2300.

[9] S. Monica and G. Ferrari, "UWB-based localization in large indoor scenarios: optimized placement of anchor nodes," *IEEE Transactions on Aerospace and Electronic Systems*, vol. 51, no. 2, pp. 987–999, April 2015.

[10] C. Gentner, M. Ulmschneider, and T. Jost, "Cooperative simultaneous localization and mapping for pedestrians using low-cost ultra-wideband system and gyroscope," in *Proceedings of IEEE/ION Position Location and Navigation Symposium*, April 2018, pp. 1197–1205.

[11] M. Driusso, C. Marshall, M. Sabathy, F. Knutti, H. Mathis, and F. Babich, "Indoor positioning using LTE signals," in *Proceedings of International Conference on Indoor Positioning and Indoor Navigation*, October 2016, pp. 1–8.

[12] M. Ulmschneider and C. Gentner, "Multipath assisted positioning for pedestrians using LTE signals," in *Proceedings of IEEE/ION Position, Location, and Navigation Symposium*, April 2016, pp. 386–392.

[13] A. Abdallah, K. Shamaei, and Z. Kassas, "Indoor positioning based on LTE carrier phase measurements and an inertial measurement unit," in *Proceedings of ION GNSS Conference*, September 2018, pp. 3374–3384.

[14] A. Abdallah, K. Shamaei, , and Z. Kassas, "Performance characterization of an indoor localization system with LTE code and carrier phase measurements and an IMU," in *Proceedings of International Conference on Indoor Positioning and Indoor Navigation*, October 2019, accepted.

[15] Z. Kassas, J. Khalife, K. Shamaei, and J. Morales, "I hear, therefore I know where I am: Compensating for GNSS limitations with cellular signals," *IEEE Signal Processing Magazine*, pp. 111–124, September 2017.

[16] K. Shamaei, J. Khalife, and Z. Kassas, "Exploiting LTE signals for navigation: Theory to implementation," *IEEE Transactions on Wireless Communications*, vol. 17, no. 4, pp. 2173–2189, April 2018.

[17] K. Shamaei, J. Khalife, and Z. Kassas, "Pseudorange and multipath analysis of positioning with LTE secondary synchronization signals," in *Proceedings of Wireless Communications and Networking Conference*, April 2018, pp. 286–291.

[18] K. Shamaei and Z. Kassas, "LTE receiver design and multipath analysis for navigation in urban environments," *NAVIGATION, Journal of the Institute of Navigation*, vol. 65, no. 4, pp. 655–675, December 2018.

[19] K. Shamaei, J. Morales, and Z. Kassas, "Positioning performance of LTE signals in Rician fading environments exploiting antenna motion," in *Proceedings of ION GNSS Conference*, September 2018, pp. 3423–3432.

[20] K. Shamaei, J. Morales, and Z. Kassas, "A framework for navigation with LTE time-correlated pseudorange errors in multipath environments," in *Proceedings of IEEE Vehicular Technology Conference*, 2019, pp. 1–6.

[21] Z. Kassas, J. Morales, K. Shamaei, and J. Khalife, "LTE steers UAV," *GPS World Magazine*, vol. 28, no. 4, pp. 18–25, April 2017.

[22] K. Shamaei, , and Z. Kassas, "Sub-meter accurate UAV navigation and cycle slip detection with LTE carrier phase," in *Proceedings of ION GNSS Conference*, September 2019, accepted.

[23] C. Gentner, E. Munoz, M. Khider, E. Staudinger, S. Sand, and A. Dammann, "Particle filter based positioning with 3GPP-LTE in indoor environments," in *Proceedings of IEEE/ION Position, Location and Navigation Symposium*, April 2012, pp. 301–308.

[24] S. Draganov, M. Harlacher, L. Haas, M. Wenske, and C. Schneider, "Synthetic aperture navigation in multipath environments," *IEEE Wireless Communications*, vol. 18, no. 2, pp. 52–58, April 2011.

[25] A. Broumandan, J. Nielsen, and G. Lachapelle, "Enhanced detection performance of indoor GNSS signals based on synthetic aperture," *IEEE Transactions on Vehicular Technology*, vol. 59, no. 6, pp. 2711–2724, July 2010.

[26] S. Daneshmand, A. Broumandan, N. Sokhandan, and G. Lachapelle, "GNSS multipath mitigation with a moving antenna array," *IEEE Transactions on Aerospace and Electronic Systems*, vol. 49, no. 1, pp. 693–698, January 2013.

[27] K. Shamaei, J. Khalife, S. Bhattacharya, and Z. Kassas, "Computationally efficient receiver design for mitigating multipath for positioning with LTE signals," in *Proceedings of ION GNSS Conference*, September 2017, pp. 3751–3760.

[28] Z. Chen, G. Gokeda, and Y. Yu, *Introduction to Direction-of-arrival Estimation*. Artech House, 2010.

[29] R. Schmidt, "Multiple emitter location and signal parameter estimation," *IEEE Transactions on Antennas and Propagation*, vol. 34, no. 3, pp. 276–280, March 1986.

[30] A. Abdallah and Z. Kassas, "Evaluation of feedback and feedforward coupling of synthetic aperture navigation with LTE signals," in *Proceedings of IEEE Vehicular Technology Conference*, 2019.

[31] R. Roy and T. Kailath, "ESPRIT-estimation of signal parameters via rotational invariance techniques," *IEEE Transactions on Acoustics, Speech, and Signal Processing*, vol. 37, no. 7, pp. 984–995, July 1989.

[32] S. Pillai and B. Kwon, "Forward/backward spatial smoothing techniques for coherent signal identification," *IEEE Transactions on Acoustics, Speech, and Signal Processing*, vol. 37, no. 1, pp. 8–15, January 1989.

[33] M. Wax and I. Ziskind, "Detection of the number of coherent signals by the MDL principle," *IEEE Transactions on Acoustics, Speech, and Signal Processing*, vol. 37, no. 8, pp. 1190–1196, August 1989.

[34] W. Pan, "Akaike's information criterion in generalized estimating equations," *Biometrics*, vol. 57, no. 1, pp. 120–125, March 2001.

[35] J. Rissanen, "Modeling by shortest data description," *Automatica*, vol. 14, no. 5, pp. 465–471., September 2019.

[36] Z. Kassas and T. Humphreys, "Observability analysis of collaborative opportunistic navigation with pseudorange measurements," *IEEE Transactions on Intelligent Transportation Systems*, vol. 15, no. 1, pp. 260–273, February 2014.